The Astrophysical Journal, 863:85 (9pp), 2018 August 10 https://doi.org/10.3847/1538-4357/aad091

Time Variability of Equivalent Width of 6.4 keV Line from the Arches Complex: Reflected X-Rays or Charged Particles?

D. O. Chernyshov[1], C. M. Ko[2], R. A. Krivonos[3], V. A. Dogiel[1], and K. S. Cheng[4]
[1] I.E. Tamm Theoretical Physics Division of P.N. Lebedev Institute of Physics, 119991 Moscow, Russia; chernyshov@dgap.mipt.ru
[2] Institute of Astronomy, Department of Physics and Center for Complex Systems, National Central University, Zhongli District, Taoyuan City 320, Taiwan, ROC; cmko@astro.ncu.edu.tw
[3] Space Research Institute of the Russian Academy of Sciences, Profsoyuznaya Str. 84/32, 117997 Moscow, Russia
[4] Department of Physics, University of Hong Kong, Pokfulam Road, Hong Kong, People's Republic of China
Received 2018 April 4; revised 2018 June 25; accepted 2018 June 29; published 2018 August 13

Abstract

Molecular gas in the Arches cloud located near the Arches cluster is one of the emitters of the K-α line of neutral iron and the X-ray continuum in the Galactic center (GC). Similarly to the cloud Sgr B2, another well-known emitter of the iron line in the GC, the Arches cloud demonstrates a temporal decline of the X-ray emission. The most natural origin of this emission is irradiation of primary photons of an X-ray flare from a distant source, most likely Sgr A*. However, recent observations of the Arches cloud discovered variations of equivalent width of the 6.4 keV iron line, which indicated that the X-ray emission from the cloud is a combination of two components with different origins and different equivalent widths, one of which is time variable, while the other is stationary during the period of observations. We considered two different scenarios: (a) this emission is formed by reflection from two clouds, which are at some distance from each other, when they are irradiated by two different flares; and (b) the other scenario assumes a combination of X-ray fluxes produced in the same cloud by reflection of primary photons and by subrelativistic cosmic rays. We present restrictions for both the model and conditions at which these scenarios can be realized. Although none of the models can be completely ruled out, we find that the X-ray reflection model requires fewer assumptions and therefore is the most viable.

Key words: cosmic rays – Galaxy: center – ISM: clouds – X-rays: ISM

1. Introduction

X-ray emission from molecular clouds was detected by the GRANAT team in 1993 (see Sunyaev et al. 1993). They assumed that this emission was the Compton echo from molecular clouds that reflected X-ray photons ejected in the past by the central source Sgr A*. They also predicted that a flux of the 6.4 keV K-α iron line had to be observed in the direction of these clouds and that the continuum and the line emission had to be time variable with a characteristic period needed for a photon front to cross the clouds. Later, these effects were observed by next-generation X-ray telescopes such as *ASCA* and *Suzaku* (Koyama et al. 1996; Nobukawa et al. 2011; Ryu et al. 2013), *INTEGRAL* (Revnivtsev et al. 2004; Terrier et al. 2010), *Chandra* (Clavel et al. 2013), and *XMM-Newton* and *NuSTAR* (Ponti et al. 2010; Clavel et al. 2014; Zhang 2015; Krivonos et al. 2017). All of these observations can be perfectly described by introducing several X-ray flares emitted by Sgr A* in the past.

It is difficult to reproduce these phenomena using charged-particle models. Indeed, charged particles are scattered by interstellar turbulence and their propagation resembles diffusion. Therefore, even if the source of the particles is transient, characteristic emission time is determined by the longer of the two timescales: (i) their propagation time from the source to the emitting cloud, and (ii) their lifetime in the medium due to energy losses. Since all phenomena mentioned above are characterized by a rapid temporal variability of the emission with a timescale of the order of several years, it is obvious that protons with very long lifetimes can be safely ruled out.

Subrelativistic electrons responsible for the X-ray emission, on the other hand, are subject to very intense energy losses. Therefore, they potentially can reproduce observed temporal variations of the emission (Yusef-Zadeh et al. 2013). However, to do so it is necessary to assume that there are several transient sources of electrons located near the X-ray emitting clouds (Dogiel et al. 2014). This situation is not impossible, but it is exceptional. Indeed, in the case of the X-ray reflection scenario, we need to set only the temporal characteristics of the source of the flares, while for the scenario with electrons we also need to assume temporal and spatial positions for the sources of the electrons. Therefore, models with subrelativistic electrons could be considered less viable.

However, the question arises whether the level of the continuum and the 6.4 keV line emission drops to zero when the photon front has left a cloud or there is a background emission generated by any other process. This emission can also be produced by the bremsstrahlung of cosmic rays (CRs) and by the K-α vacancy production in iron atoms by subrelativistic electrons or protons (see, e.g., Dogiel et al. 1998; Tatischeff 2003). Attempts to interpret the generation of the continuum and line emission from the clouds by CRs were undertaken in several models (see, e.g., Yusef-Zadeh et al. 2002, 2013; Dogiel et al. 2009, 2011; Tatischeff et al. 2012). However, the clearly observed time variability of X-ray fluxes from the clouds was completely unfavorable to these models (see, e.g., Dogiel et al. 2014).

Although subrelativistic CRs (unlike relativistic CRs) do not produce visible radiation fluxes that could be detected in the Galaxy, there are indications that their density is not zero in the interstellar medium. Thus, the observed ionization of interstellar hydrogen may be produced by subrelativistic CRs (see Indriolo & McCall 2012; Dogiel et al. 2013), and the estimated energy density in the central molecular zone region could be as high as 100 eV cm^{-3} (see Yusef-Zadeh et al. 2007; Tatischeff et al. 2012; Dogiel et al. 2015). Therefore, a nonzero flux of

X-rays from the clouds is expected when the front of primary photons has left it. Attempts to estimate this flux from the cloud Sgr B2 were undertaken in Dogiel et al. (2014, 2015). According to their result, the present 6.4 keV flux from this cloud is close to the expected stationary level, but these estimates cannot be considered reliable. There is no confirmation from observations that the Sgr B2 6.4 keV flux has reached its stationary minimum, although its value has decreased by more than one order of magnitude from the peak. Observations by Zhang (2015) suggested a possibility that the stationary component started to appear, but reliable results from further observations are necessary.

Interesting effects of X-ray variability were recently observed in the direction of the Arches cluster by Krivonos et al. (2017). The Arches cluster is a cluster of young massive stars in the Galactic center (GC). It is likely associated with the "$-30\,\mathrm{km\,s^{-1}}$" molecular cloud. The mass of the cloud is estimated to be $\sim 6 \times 10^4\,M_\odot$, the hydrogen density there is about $n_\mathrm{H} \simeq 10^4\,\mathrm{cm^{-3}}$, the gas column density is $N_{\mathrm{H}_2} \simeq 4 \times 10^{23}\,\mathrm{cm^{-2}}$, and the radius is about 3 pc (Serabyn & Guesten 1987). Continuum and 6.4 keV line X-ray emission was found in the direction of the cloud by Yusef-Zadeh et al. (2002) and Wang et al. (2006). The line emission from the cloud varies with time (Clavel et al. 2014) and is also characterized by a relatively high equivalent width; therefore, its origin is most likely due to the reflection of primary photons emitted by an external source.

Recently, Krivonos et al. (2017) found time variations of the continuum in the range 2–10 keV and the line 6.4 keV emission. The essential result of this observation is that they also found time variations of the line equivalent width (eW) from 0.9 ± 0.1 keV in 2007 to 0.6–0.7 keV in 2015. This means that the Arches emission is a mixture of two components with different equivalent widths. For certain, the time-variable component observed by Krivonos et al. (2017) can be interpreted as the Thomson scattering of primary photons, e.g., from Sgr A*, that are leaving this complex. The second component can be due to either the Thomson scattering of photons from another molecular complex that is at a large enough distance from Arches but is on exactly the same path of view or due to a contribution of CRs in the total X-ray flux. In both cases, the effect of eW time variability is naturally expected. In Section 2, we discuss both interpretations.

2. Input Parameters of the X-Ray Emission for the Stationary and Time-varying Components

As follows from Krivonos et al. (2017), the flux of the 6.4 keV line was constant for the period 2002–2007 and equal to $I_0 = 8.84$ in units of 10^{-6} ph s^{-1} cm^{-2}. After 2007, this flux was decaying at a rate of $\alpha = 0.64$ yr^{-1} in the same units.

We assume that this flux consists of two components: a time-variable component C_{XR} produced by primary photons from an external source that decays with time when $t \geqslant t_0$, i.e., when the front of primary photons leaves the cloud, and a stationary component C_{C2} of unknown origin. We expect that at unknown time t_X this flux has reached the background stationary level of the 6.4 keV flux C_{C2} when the front of primary photons left the cloud. These temporal variations can be presented from Krivonos et al. (2017) as

$$\frac{I_{6.4}(t)}{10^{-6}\ \mathrm{ph\ s^{-1}\ cm^{-2}}} = \begin{cases} C_{C2} + C_{\mathrm{XR}} & \text{if } t \leqslant t_0 \\ C_{C2} + C_{\mathrm{XR}} - \alpha(t - t_0) & \text{if } t_0 < t < t_\mathrm{X}, \\ C_{C2} & \text{if } t \geqslant t_\mathrm{X} \end{cases} \quad (1)$$

where $t_0 \approx 2007.4$ years and C_{XR} is the unknown contribution of a varying X-ray component in the 6.4 keV flux from Arches. The unknown time t_X can be estimated as $t_\mathrm{X} = t_0 + C_{\mathrm{XR}}\alpha^{-1}$, if C_{XR} is known.

It is natural to assume that the continuum emission $I_\mathrm{X}(E_\mathrm{X})$ produced by primary X-ray photons evolves in the same way as 6.4 keV line emission. We also assume that each of these components is characterized by a different equivalent width of the 6.4 keV line, $\mathrm{eW}_{\mathrm{XR}}$ and eW_{C2}, which do not equal each other, $\mathrm{eW}_{\mathrm{XR}} \neq \mathrm{eW}_{C2}$, and remain constant in time. Here,

$$\mathrm{eW} = \frac{I_{6.4}}{I_\mathrm{X}(E_\mathrm{X} - 6.4\ \mathrm{keV})}. \quad (2)$$

Then, the total eW in the time interval $t_0 < t < t_\mathrm{X}$ can be presented as

$$\mathrm{eW} = \frac{C_{C2} + C_{\mathrm{XR}} - \alpha(t - t_0)}{\mathrm{eW}_{\mathrm{XR}}^{-1}[C_{\mathrm{XR}} - \alpha(t - t_0)] + \mathrm{eW}_{C2}^{-1}C_{C2}}. \quad (3)$$

From Krivonos et al. (2017) we have $\mathrm{eW}(t = t_0) = \mathrm{eW}_0 = 0.9 \pm 0.1$ keV, while at $t_1 = t_0 + \Delta t$, where $\Delta t = 9$ years, $\mathrm{eW}(t = t_1) = \mathrm{eW}_1 = 0.65 \pm 0.06$ keV. Then, Equation (3) gives

$$\mathrm{eW}_{\mathrm{XR}} = \frac{\alpha(t_1 - t_0)}{\mathrm{eW}_0^{-1}(C_{\mathrm{XR}} + C_{C2}) - \mathrm{eW}_1^{-1}(C_{\mathrm{XR}} + C_{C2} - \alpha\Delta t)}$$
$$\mathrm{eW}_{\mathrm{XR}} = \frac{I_{6.4}(t_0) - I_{6.4}(t_0 + \Delta t)}{\mathrm{eW}_0^{-1}I_{6.4}(t_0) - \mathrm{eW}_1^{-1}I_{6.4}(t_0 + \Delta t)} = 1.1 \pm 0.3\ \mathrm{keV}. \quad (4)$$

Two conclusions follow from this result. For solar abundance the equivalent width of the line generated by photons is (see Tsujimoto et al. 2007)

$$\mathrm{eW}_{\mathrm{XR}}^{\mathrm{solar}} \approx 3\left(\frac{1}{\Gamma + 2}\right)\left(\frac{6.4}{7.1}\right)^{\Gamma}\left(\frac{1}{1 + \cos^2\theta}\right)\mathrm{keV}, \quad (5)$$

where Γ is the spectral index of primary photons and θ is the reflection angle. For estimates we take $\theta \approx \frac{\pi}{2}$. From this equation one can obtain that $\mathrm{eW}_{\mathrm{XR}}^{\mathrm{solar}} = 0.7$ keV for the spectrum of the X-ray continuum $\Gamma = 1.6$ derived by Krivonos et al. (2017). Then, from Equation (4) it follows that $\mathrm{eW}_{\mathrm{XR}} = \eta\mathrm{eW}_{\mathrm{XR}}^{\mathrm{solar}}$ (η is the iron abundance relative to the Sun) and it gives $\eta = 1.6 \pm 0.4$ in Arches, which is the same as derived by Tatischeff et al. (2012).

The other conclusion is that $\mathrm{eW}_{\mathrm{XR}} > \mathrm{eW}_0$, i.e., even at times $t \leqslant t_0$ the contribution of stationary component into the total continuum and line fluxes is nonzero.

As a next step we try to estimate the contribution of stationary component C_{C2}, accepting that the spectral index of the variable X-ray components equals $\Gamma = 1.6$ and does not

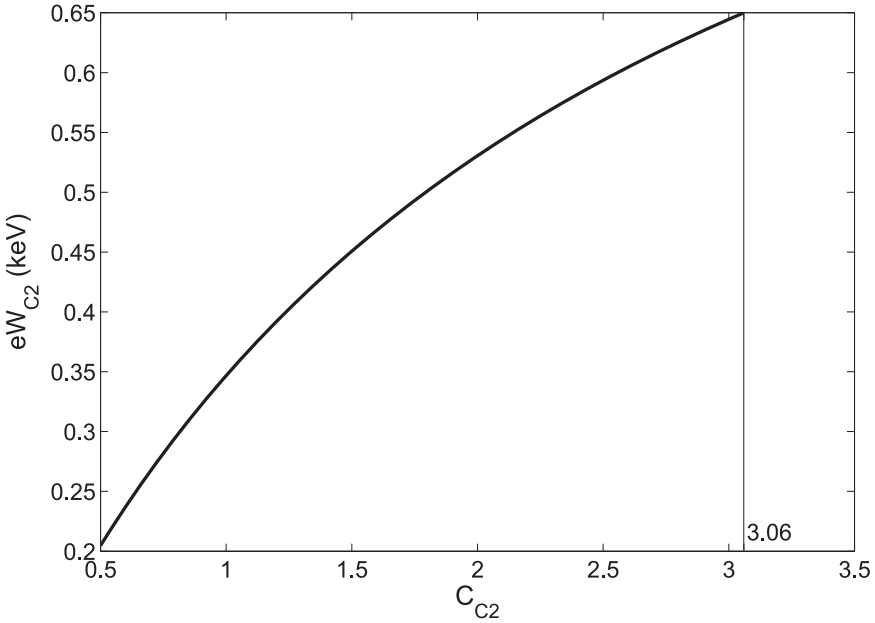

Figure 1. Equivalent width of the stationary component as a function of its normalization. Here, the Arches iron abundance equals 1.6 of solar and $C_{C2} < 3.06$.

change in time. For the given spectral index Γ, eW_{C2} cannot exceed $\mathrm{eW}_1 = 0.65 \pm 0.06$ keV, which gives the upper limit for C_{C2}, $C_{C2} < 3.06$.

Then, the 6.4 keV line intensity can be presented from Equations (2) and (3) as

$$\mathrm{eW}_{C2} = \frac{\mathrm{eW}_0 C_{C2}}{I_{6.4}(t_0) - \frac{\mathrm{eW}_0}{\mathrm{eW}_{\mathrm{XR}}}[I_{6.4}(t_0) - C_{C2}]}. \quad (6)$$

The function $\mathrm{eW}_{\mathrm{CR}}(C_{C2})$ is shown in Figure 1. As one can see, equivalent width can be as high as 0.65 keV for $C_{C2} = 3.06$.

Since the abundance of iron in Arches cluster is not fixed well, for theoretical estimations we use the solar abundance of iron $n_{\mathrm{Fe}}/n_{\mathrm{H}} = 3 \times 10^{-5}$ (Tsujimoto et al. 2007) as a reference value. The corresponding values of equivalent width for iron abundance of 1.6 solar can be obtained by multiplication of solar abundance value by a factor of 1.6. For example, in order to reproduce the aforementioned equivalent width of 0.63 keV in the Arches environment we need to obtain a value of about 0.3–0.5 keV for the solar abundance.

We notice that Tatischeff et al. (2012), using a high-quality *XMM-Newton* data set, measured the spectral index of the X-ray emission from the Arches cloud as $\Gamma_{\mathrm{X}} = 1.6^{+0.3}_{-0.2}$, later confirmed by Krivonos et al. (2014) with *NuSTAR* in 2012 ($\Gamma_{\mathrm{X}} = 1.6 \pm 0.3$). Subsequent *NuSTAR* observations of the Arches cluster complex showed the trend of softening of the non-thermal power-law continuum. Krivonos et al. (2017) determined $\Gamma_{\mathrm{X}} \sim 2$ in 2015 observations, and a recent analysis of the *NuSTAR* data acquired in 2016 showed $\Gamma_{\mathrm{X}} = 2.7 \pm 0.5$ (E. Kuznetsova et al. 2018, in preparation); however, the uncertainties are large. Summarizing the above, we define that allowed values of the spectral index, following from observations, are within the limits

$$1 \leqslant \Gamma_{\mathrm{X}} \leqslant 2. \quad (7)$$

We also notice that these results permit a time variability of Γ_{X} within the limits during the period of observations.

3. Parameters of of the X-Ray Emission Created by an Additional X-Ray Flare

As we mentioned above, eW of the reflected X-ray emission depends on the following parameters: the spectral index of the primary flare, the reflection angle, and the abundance of iron (see Equation (5)).

The most straightforward way to interpret these variations is to assume changes of the iron abundance in the complex when the front is moving along it. However, since X-ray emission does not show significant spatial offset (Krivonos et al. 2017), we find it highly unlikely that two components of the same complex have completely different chemical compositions.

Another explanation is to assume that two separated molecular complexes are irradiated by the same or by two different X-ray flares of an external X-ray source when the front of X-rays is inside the cloud during the entire time of the observation that provides the stationary component C_{C2}, while this (or the other) front is leaving the second cloud that provides the time-variable component C_{XR}. If the spatial separation between these clumps is large enough, they are irradiated at different reflection angles, θ_{C2} and θ_{XR}, that mimic the temporal variability of the total equivalent width eW. Possible reflection geometry is shown in Figure 2.

In the Thomson regime, one can relate the reflection angles in the following way:

$$\cos^2\theta_{C2} = \frac{\mathrm{eW}_{\mathrm{XR}}}{\mathrm{eW}_{C2}}(1 + \cos^2\theta_{\mathrm{XR}}) - 1. \quad (8)$$

The right-hand side of the equation is smaller than unity, which gives $\mathrm{eW}_{C2} < 0.5\mathrm{eW}_{\mathrm{XR}}$. From Figure 1 we conclude that $C_{C2} \geqslant 2$.

If primary photons are generated by the same external source, then the separation distance between the complexes

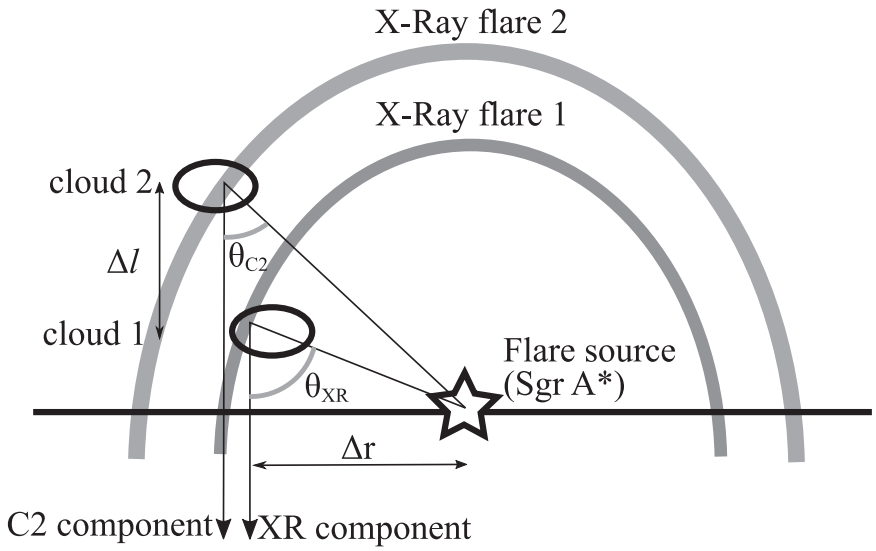

Figure 2. Positions of the two clouds and possible reflection geometry.

along the line of sight Δl can be presented as

$$\Delta l = \Delta r \left\{ \left[\frac{2 - \frac{\mathrm{eW_{XR}}}{\mathrm{eW_{C2}}}(1 + \cos^2\theta_{\mathrm{XR}})}{\frac{\mathrm{eW_{XR}}}{\mathrm{eW_{C2}}}(1 + \cos^2\theta_{\mathrm{XR}}) - 1} \right]^{-0.5} - \tan^{-1}\theta_{\mathrm{XR}} \right\}, \quad (9)$$

where $\Delta r = 25$ pc (see, e.g., Yusef-Zadeh et al. 2002) is the projected distance between the source of the X-ray flare (hereafter, we assume it is Sgr A*) and emitting cloud. Here, we assume that both components are located either closer to us than Sgr A* or behind it. If $\frac{\mathrm{eW_{XR}}}{\mathrm{eW_{C2}}} \approx 1.52$, the spatial separation reaches the minimum value of $\Delta l = 25$ pc for $\theta_{\mathrm{XR}} \approx 0.45\pi$. Since the size of the Arches complex is about 6 pc, the reflection regions belong to different molecular clouds.

From the equation for temporal delay, Δt_{XR}, of the Compton echo for the *XR* component (see, e.g., Sunyaev & Churazov 1998)

$$\frac{\Delta l}{c} = \frac{1}{2\Delta t_{\mathrm{XR}}}\left[\Delta t_{\mathrm{XR}}^2 - \left(\frac{\Delta r}{c}\right)^2\right], \quad (10)$$

which gives for $\theta_{\mathrm{XR}} \approx 0.45\pi$ the temporal delay of about $\Delta t_{\mathrm{XR}} = 100$ years, which is in good agreement with the findings of Churazov et al. (2017) and Chuard et al. (2018), who estimated the age of the X-ray flare to be about 110 years.

The second component should have a reflection angle of $\theta_{C2} = 0.23\pi$, and the temporal delay in this case is about $\Delta t_{\mathrm{CR}} = 230$ years. It is highly unlikely that both of these components were created by the same flare, since according to Churazov et al. (2017) the duration of the 110 year old one is of the order of several years. It is more reasonable to assume for this scenario that there are two clouds located on the same line of sight that are irradiated by two successive X-ray flares separated by about 130 years. We note that the timings of these two flares are in very good agreement with so-called two-event scenario for X-ray emission from the GC (Clavel et al. 2013; Walls et al. 2016; Terrier et al. 2018). A similar scenario was derived by Chuard et al. (2018) from the *XMM-Newton* and *Chandra* data; they found from their analysis two flares of Sgr A*: 110 and 240 years ago. According to Clavel et al. (2013) the older flare should be at least several decades long. Therefore, this flare may be responsible for the stationary component C_{C2}.

Above, we assumed that the Arches cloud is located farther away than Sgr A*. If it is located closer to us, temporal delays for given reflection angles should be the following: $\Delta t_{\mathrm{XR}} =$ 74 years and $\Delta t_{C2} = 33$ years. The value of Δt_{C2} is too low, so we consider this situation to be unlikely.

Relative positions of the clouds can be roughly estimated based on their absorption column density $N_{\mathrm{H_2}}$. Observations indicate that there is a slight decrease of absorption column density with time: it drops from 7×10^{22} cm^{-2} (Clavel et al. 2014) to slightly below 7×10^{22} cm^{-2} (Krivonos et al. 2017). This implies that the cloud responsible for component *C*2 absorbed less than the first one. This may indicate that the second cloud is actually located closer to us, but we do not really know what fraction of $N_{\mathrm{H_2}}$ came from absorption in the medium located near the cloud or within the cloud itself (i.e., a local effect) and not related to actual distance. Indeed, for other molecular clouds in the GC described by Ponti et al. (2010) the absorption column density is 4×10^{22} cm$^{-2} \leqslant N_{\mathrm{H_2}} \leqslant 10 \times 10^{22}$ cm^{-2}. The Arches cloud is within this range.

The total luminosity of the 230 year old flare in the energy range 1–10 keV can be estimated to be (Sunyaev & Churazov 1998)

$$L_{C2}^{X} \approx 6 \times 10^{38}\ \mathrm{erg\ s^{-1}} \left(\frac{C_{C2}}{3}\right)\left(\frac{M_{C2}}{10^3 M_\odot}\right)^{-1}\left(\frac{\eta}{1.6}\right)^{-1}, \quad (11)$$

where M_{C2} is mass of the cloud irradiated by the flare, $M_\odot$ is the solar mass, and η is the iron abundance relative to the solar. Luminosity of the flare necessary to illuminate Sgr B2 is $L_{\mathrm{SgrB2}}^{X} \approx 10^{39}$ erg s^{-1} (Koyama et al. 1996). One can see that the assumption of the 230 year old flare is indeed the same one that illuminates Sgr B2 and can be justified for reasonable values of the mass of the clump. Indeed, given the size of the emitting region of about $a \times b = 1$ pc$\times$ 2.3 pc and the absorption column density of $N_{\mathrm{H_2}} = 7 \times 10^{22}$ cm^{-2} (Krivonos et al. 2017), one can estimate an upper limit of the total

irradiated mass as

$$M_{C2} \leqslant \pi ab \cdot m_p \cdot N_{\rm H_2} \approx 3.7 \times 10^3 M_\odot, \quad (12)$$

and therefore each of the two components passes through $1.8 \times 10^3 M_\odot$ of molecular gas. Note that actual sizes and actual values of $N_{\rm H_2}$ related to clouds should be different. Therefore, the value obtained above should only be used as a rough estimate.

The only difficulty of this model is that this scenario requires coincidence of very specific conditions when the two complexes are exactly on the line of sight and they are separated exactly by a distance of 25 pc.

4. Spectral Parameters of the X-Ray Emission Created by Charged Particles

4.1. Basic Equations for the Emission Created by Charged Particles

We assume that the spectrum of primary charged particles (protons or electrons) inside the molecular cloud is a power law. Besides, *Fermi*-LAT has not found a gamma-ray flux from Arches at a level above 10^{-5} ph cm^{-2} s^{-1}. It means that there should be significant steepening in the the relativistic energy range of the CR spectrum associated with the Arches cluster. The simplest way is to introduce an effective cutoff at the energy $E_{\rm max}$ that is below the limit of 100 MeV photon production. For protons we can set it below the threshold of the $p-p$ reaction, i.e., $E_{\rm max} \leqslant$ 200–300 MeV, while for electrons we can take $E_{\rm max} \leqslant$ 100 MeV. Then, for the spectrum of CRs penetrating from outside we take it in the form

$$f_{p,e}(E) = AE^{\delta} \cdot \Theta(E_{\rm max} - E), \quad (13)$$

where A is a normalization constant, $\Theta(E)$ is the Heaviside function, and the spectral index δ and the maximum energy $E_{\rm max}$ are parameters of the model.

CRs penetrating from outside generate secondary electrons in the Arches cloud that also contribute to the total X-ray flux from there. For the stationary model the spectrum of secondary electrons can be derived from

$$\frac{\partial}{\partial E}\left(\frac{dE}{dt} f_{\rm se}\right) = Q_{\rm se}(E), \quad (14)$$

where $f_{\rm se}(E)$ is the volume-averaged distribution function of secondary particles, $\frac{dE}{dt}$ describes energy losses by ionization and bremsstrahlung (Blumenthal & Gould 1970), and the term $Q_{\rm se}(E)$ describes the production spectrum of secondary particles,

$$Q_{\rm se}(E) = n \int dE_p f_p(E_p) v \left(\frac{d\sigma(E_p, E)}{dE}\right)_{\rm se}. \quad (15)$$

Here, $(d\sigma/dE)_{\rm se}$ is the cross-section of electron production by the knock-on process (Hayakawa 1964). Electrons produced by proton–proton collisions can be safely ignored since we only consider protons with energies below the threshold of pion production. The rate of energy losses, $\frac{dE}{dt}$, and the production function of electrons, $Q_{\rm se}(E)$, in Equation (14) are proportional to the ambient density, n. Therefore, the resulting spectrum of secondary electrons, $f_{\rm se}$, is independent of this medium parameter. We ignore the escape of secondary electrons from the cloud because their lifetime inside the dense cloud is quite short.

For the known distribution functions of protons, $f_p(E)$, and electrons, $f_e(E)$ and $f_{\rm se}(E)$, the spectrum of the X-ray continuum can be estimated to be

$$I_x(E_x) = n \sum_{p,e} \int dE\, f_{p,e}\, v \left(\frac{d\sigma(E, E_x)}{dE_x}\right)_{\rm br}, \quad (16)$$

where $\left(\frac{d\sigma(E, E_x)}{dE_x}\right)_{\rm br}$ is the cross-section of inverse-bremsstrahlung emission for protons and of bremsstrahlung emission for leptons (Blumenthal & Gould 1970). We take also into account electron–electron bremsstrahlung (Haug 1998) whose contribution is significant for the hard spectra of electrons. Indeed, as one can see from Haug (1998), 10 MeV electrons produce about 1.5 times more 6.4 keV photons through electron–electron in comparison to electron–proton bremsstrahlung.

The intensity of the 6.4 keV line is estimated to be

$$I_{6.4} = n\eta \sum_{p,e} \int dE\, f_{p,e}\, v \sigma_{\rm Fe}^{\rm K\alpha}, \quad (17)$$

where η is a relative abundance of the iron atoms on the cloud and $\sigma_{\rm Fe}^{\rm K\alpha}$ is a cross-section of the production of 6.4 keV photon by proton and electron impact (see Tatischeff 2003).

When the intensity of the X-ray emission is known, it is possible to estimate the total power in charged particles (protons or electrons) required to produce this emission. The difference between protons or electrons is about a few since their cross-sections for producing X-ray photons are of the same order (Tatischeff 2003). The luminosity of the source of charged particles estimated by Tatischeff et al. (2012) is about $\sim 10^{39}$ erg s^{-1}.

Another important parameter of X-ray emission following from observation is the steepening of its spectrum above 10 keV. According to Krivonos et al. (2017), the X-ray spectrum is steepening from $\Gamma_{\rm X} = 1.6$ at $E_{\rm X} < 10$ keV to $\Gamma_{\rm X} = 2$ at higher energies. This spectral change can be reproduced by introducing a spectral break $E_{\rm br} \approx 200$ MeV for protons (that is about the required value of $E_{\rm max}$) and at $E_{\rm br} \approx 100$ keV for electrons.

4.2. Pure Hadronic and Leptonic Models with a Stationary Spectral Index

Here, we assume that the spectral index of X-ray emission produced by CRs (stationary component) equals exactly that of X-ray emission generated by an external source (variable component). For the allowed range of $\Gamma_{\rm X}$ (see Equation (7)) one can estimate from Equations (16) and (17) the equivalent width of the 6.4 keV line eW$_{C2}$ generated by CRs. The result $\eta = 1$ is shown in Figure 3 by the solid lines where we plotted equivalent width as a function of the spectral index of X-ray emission $\Gamma_{\rm X}$ between 1 and 7 keV. The curves at the top right corner show the function eW($\Gamma_{\rm X}$) for protons and the curves at the bottom for electrons. These curves define the background level of eW for the case of protons or electrons, when the X-ray front has left the cloud. Each curve corresponds to different $E_{\rm max}$: we used values of 50 MeV $\leqslant E \leqslant$ 3 GeV for protons, and we used values of 100 keV $\leqslant E \leqslant$ 3 MeV for electrons. One can see that equivalent width weakly depends on the value of $E_{\rm max}$. The minimum allowed value of $\Gamma_{\rm X}$, however, depends on $E_{\rm max}$, and therefore it is unlikely to generate X-ray emission

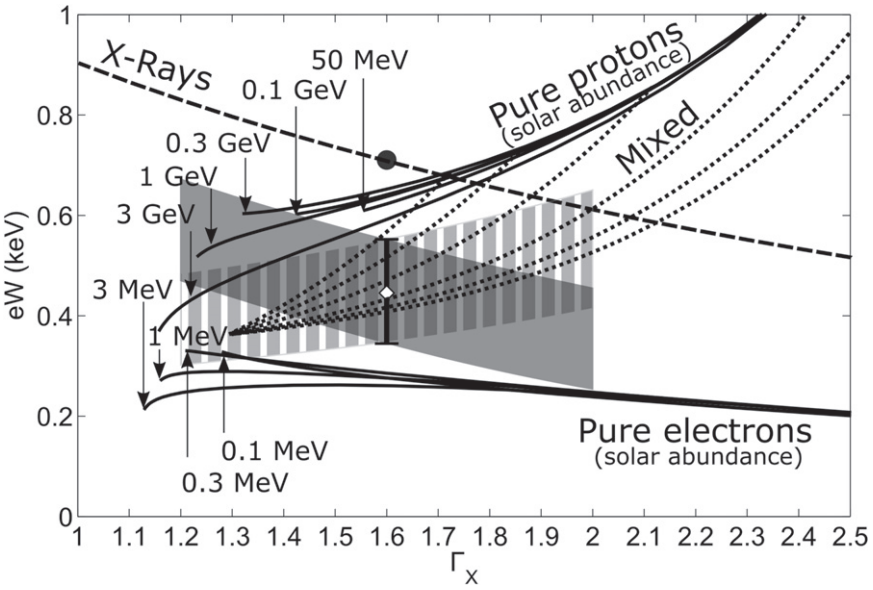

Figure 3. Equivalent width as a function of spectral index of the X-ray emission produced by charged particles or photons in the energy range between 1 and 7 keV. Solid lines correspond to pure hadronic models (top curves) and pure leptonic models (bottom curves) with different values of maximum energy E_{max}. Dashed line corresponds to the emission produced by primary X-rays. Dotted curves correspond to mixed (hadronic plus leptonic) models with different fractions of components. Data points in the middle—equivalent width at 2015 calculated in Section 2. Gray area—possible variations of the experimental value of equivalent width in the case of if the spectral index of the emission is different from $\Gamma = 1.6$: solid area—if the spectral index of the X-ray emission does not vary with time, striped area—if the spectral index of the X-ray emission is not constant. Black dot corresponds to the time-varying component prior to 2007. Solar abundance of iron is assumed.

with a hard spectrum by protons ($\Gamma_X < 1.6$) if their maximum energy is below $E_{max} < 40$ MeV.

Curves with high values of E_{max} are included in Figure 3 for the sake of generality. Indeed, relativistic particles should generate a prominent flux in gamma-rays. For example, for $E_{max} = 3$ GeV and the minimum value of Γ_X corresponding to $\delta = 0.5$, the gamma-ray emission above 100 MeV is expected to be of the order of 10^{-5} ph cm^{-2} s^{-1}. Also, steepening of the X-ray spectrum above 10 keV cannot be reproduced if the spectral index of primary particles remains constant.

In Figure 3, we also plotted the equivalent width of the 6.4 keV line produced by primary X-rays. The corresponding dependence is shown by a dashed line and it represents the time-variable (C_{XR}) component of the emission observer before 2007. The value of eW derived from the *NuSTAR* data for $\Gamma_X = 1.6$ is shown by the data points in the middle of the figure. The estimated values of eW for the range of Γ_X defined by Equation (7) if it is time independent is shown in the gray area of Figure 3.

Regardless of the emission process, the value of eW is proportional to the abundance of iron. Therefore, despite absolute positions of the curves in Figure 3 that depend on the iron abundance, their relativity to each other's positions do not. With this in mind, we plotted all curves in Figure 3 assuming solar abundance of iron for convenience.

One can see that although protons can provide a drop of the equivalent width with time, the magnitude of this drop is not big enough to reproduce the results of Krivonos et al. (2017), except for the case of $E_{max} \geqslant 0.1$ GeV when the spectral index $\Gamma_X < 1.4$. Then, the theoretical curves fall into the shaded area, defining the background level produced by protons. As follows from observations of Tsujimoto et al. (2007) the X-ray continuum spectrum in Arches is indeed very hard with an index of $\Gamma_X < 1.4$, yet background contamination is possible. In addition, for $E_{max} \leqslant 0.2$ GeV spectral turnover at $E_x = 10$ keV, reported by Krivonos et al. (2017), is also reproduced. From Figure 3 one can see that in the case of the pure hadronic model, the X-ray emission in 2015 reached its background (stationary) level and was fully produced by protons, i.e., the X-ray front completely left the area of Arches.

We notice that the scenario of bombardment by low-energy protons with hard spectra may interpret the 6.4 keV production in the Sgr B2 molecular cloud (Dogiel et al. 2015) and in the Inner Galactic Ridge (Nobukawa et al. 2015).

For the pure leptonic model the situation is different. Electrons are characterized by very low equivalent width. According to Figure 1, the contribution of electrons to the total X-ray flux in the pure leptonic model should be low, and the appearance of the stationary component is expected in several years as follows from Figure 3, if it can be measured.

The problem of the electron model is their short lifetime. The lifetime of 10 keV electrons in the medium with a density of 10^4 cm^{-3} is less than 0.1 years. Penetrating from outside they can fill the shell with a thickness of about 10^{16} cm unless they are accelerated inside in situ. However, if the energy of the primary electrons is about 1 MeV, they can fill the entire volume of the cloud.

The spectrum of X-ray emission produced by electrons penetrating into molecular clouds was analyzed by Tatischeff et al. (2012). They assumed that according to Skilling & Strong (1976) low-energy electrons are excluded from the molecular clouds. Therefore, the spectrum of low-energy electrons is formed entirely by energy losses, and since at low energies ionization losses dominate, the spectrum of electrons should be very hard. As a result, the index of the X-ray spectrum produced by electrons should be low: $\Gamma_X \leqslant 1.4$

Moreover, in order to reproduce the spectral break at hard X-rays one need to assume that there is a cutoff or a hard spectral break in the spectrum of primary electrons at $E_{max} \leqslant 100$ keV. The corresponding lifetime of these electrons is about 1.4 years.

The theoretical curve for electrons is located below the shaded area. As follows from Figure 1, the stationary level of the pure leptonic model corresponds to $C_{C2} \approx 2$, i.e., should be about 1.5 times lower than observed in 2015.

Therefore, the main difference between the pure hadronic and pure leptonic models is the value of stationary level: in the case of the pure hadronic model the stationary level has already been reached, while in the case of the pure leptonic model it is still below the current observations. In both models, the spectral index of the X-ray emission should be rather hard: $\Gamma_X \approx 1.3$–1.4, which allows us to separate these CR models from the model of X-ray flares irradiating two different clouds (two Compton echoes with different equivalent widths).

4.3. Models with Temporal Variations of the Spectral Index

Above, we analyzed the case when spectral indexes of continuum X-ray emission generated by photons and charged particles equal each other. In this case, the spectral index of total emission is independent of time even if relative contributions are time varying. Such a situation is possible but exceptional. It is more natural to assume that spectral indexes of photon and the CR components differ from each other. Then, the spectral index of the total X-ray emission is a function of time, $\Gamma_X(t)$.

If we accept variations of the continuum index from $\Gamma_X = 1.6$ in 2007 to $\Gamma_X \neq 1.6$ in 2015, then values of eW of 2015 should be re-calculated. To do this, we re-evaluated the spectral model of the cloud emission (Model 2 in Table 4 in Krivonos et al. 2017) on *XMM-Newton* data acquired in 2015 to estimate eW for fixed Γ_X running in the range 1.2–2 (with a step of 0.1). The expected changes of eW for different values of Γ_X are shown in the gray area of Figure 3. One can see that curves in the proton scenario are completely unacceptable because their stationary level is higher than that measured in 2015.

The situations for electrons, as one can see from Figure 3, are similar to those described in the previous section. However, in this case, the spectral index of the variable X-ray component and that of stationary component are different, and the stationary level generated by electrons can be reached now if the spectral index of bremsstrahlung emission is about $\Gamma_X \approx 1.3$–1.4.

4.4. Mixed Models

A more realistic model should include contributions from both protons and electrons. Indeed, in shocked plasma, as was shown by Baring et al. (2000), the contribution of inverse bremsstrahlung produced by protons can be safely neglected (see, however, Nobukawa et al. 2018). However, as we move away from the source of CRs, energy losses suppress the density of electrons and a relative contribution of hadronic emission increases. Thus, we expect that both electrons and protons contribute nonzero fractions of the X-ray emission into the total stationary flux from the Arches.

We use the equations from Section 4.1 assuming the following spectra for particles. For electrons it is fully defined by losses: according to Tatischeff et al. (2012), if the spectrum of low-energy electrons injected into the cloud is hard enough (see, e.g., Skilling & Strong 1976), then inside the cloud the spectrum should satisfy the expression

$$f_e(E) = A\left(\frac{dE}{dt}\right)^{-1}\Theta(E_{\max} - E), \tag{18}$$

where $\frac{dE}{dt}$ describes energy losses experienced by electrons. As we already mentioned before, energy losses of electrons are more severe at low energies. Therefore, the spectrum of electrons obtained from Equation (18) is hard. For protons we use spectrum in the form described by Equation (13).

We consider both scenarios for stationary and time-variable spectral indexes. Equivalent widths as a function of spectral index for different proportions of electrons and protons and for different spectral indexes of protons are shown in Figure 3 as dotted lines. One can see that the combination of the hard spectrum produced by electrons and the soft spectrum produced by protons can potentially reproduce any observed equivalent width and spectral index.

Different positions on the dashed lines correspond to different ratios between electrons and protons that are varying along the curve. The bottom left end of the lines corresponds to pure leptonic models, while the point of intersection of the dashed lines and the proton lines correspond to pure hadronic models.

5. Discussion and Conclusion

We investigated two scenarios to reproduce the observed variations of equivalent width of iron Kα line observed from the direction of the Arches cluster. We assume that there is a different component of the X-ray emission that varies much slower, and therefore can be considered as stationary. The second component can be produced either by a different primary X-ray flare or by subrelativistic CRs.

The most conservative way to explain variations of equivalent width of iron Kα line is to use a two-event model proposed by Clavel et al. (2013) and recently updated by Chuard et al. (2018). There are two flares in this model that occurred in the GC: one about 100 years old and the other about 200 years old. They irradiated two different clouds on the light of view, separated by a distance $\gtrsim$25 pc. Because of different reflection scattering, irradiated emission from this cloud is characterized by different equivalent widths. The reflection angle of the older flare is smaller than that of the younger one. Therefore, it has a smaller equivalent width. As follows from the results of Section 2, we should assume that this flare is responsible for the stationary component of emission and hence the duration of these flares should be long enough.

For the timings of the flares taken from Chuard et al. (2018) the second component from the older flare should already be observed and therefore the stationary level already should be archived. However, if the timing of the second flare is different, for example, if it is older than the two reported by Chuard et al. (2018), the stationary level can be lower. However, it will require more significant spatial separation between emitting clouds, and the stationary level of the 6.4 keV line emission can be reduced only by a factor of 1.5 in comparison to the intensity observed in 2015.

Explaining the same variations by charged particles has some shortcomings but cannot be completely ruled out. If we accept variations of the X-ray spectral index within $1.3 \leqslant \Gamma_X \leqslant 2$, we arrive at the following conclusions:

1. The pure hadronic model requires a stationary X-ray spectral index of the total emission, $\Gamma_X = 1.3$, in the period from 2007 to 2015. Otherwise, the value of the equivalent width of the iron line produced by protons would be too large to reproduce the observed variations. As follows from the hadronic model, we have reached the stationary level of the X-ray emission from Arches in 2015.
2. According to Tatischeff et al. (2012), the pure leptonic model requires a hard spectral index $\Gamma_X = 1.3$ when the stationary level is attained. However, unlike the hadronic model, the stationary level of the 6.4 keV line emission may be 1.5 less than observed in 2015. Therefore, in 2015 we may still observe a combination of varying components produced by primary X-rays and a stationary component produced by electrons. In this case, the spectral index of the emission can be softer: $\Gamma_X > 1.3$. Future observations can potentially measure the spectral index more carefully and therefore restrict these models.
3. In the case of mixture of protons and electrons, the value of the spectral index is not really restricted. Therefore, it is quite difficult to distinguish between charged particles and X-rays. Information on ionization and nuclear lines (Tatischeff et al. 2012) might be essential for clarification.

The total CR power required to generate observed X-ray fluxes from Arches is about 4×10^{38}–10^{39} erg s^{-1}, which is close to the findings of Tatischeff et al. (2012). As was shown by Tatischeff et al. (2012), this power can be generated by collision between the Arches cluster and the Arches cloud. Observations show that the Arches cluster moves toward northeast in the equatorial coordinates (Stolte et al. 2008), and regions bright in the 6.4 keV line are located to the the north, east, and southeast from the cluster (Krivonos et al. 2017). Therefore, it is possible to assume that CRs are accelerated near the sites of collision between the Arches cluster and dense gas clumps.

In our analysis, we assumed that the cloud responsible for time-varying components is located in the same plane as Sgr A* and that the reflection angle is close to $\pi/2$. That resulted in a relative iron abundance of about a 1.6 solar value. This assumption, however, may be incorrect, and the cloud in question may be located closer to us or farther away, resulting in higher iron abundance necessary to reproduce the observed equivalent width. This changes in application to charged-particle models will proportionally shift the data point and the gray areas in Figure 3 downward, making electron scenarios more viable and proton scenarios less viable.

The X-ray reflection scenario is more sensitive to the assumed iron abundance. Indeed, as one can see from Equation (9), the separation between the two clouds is very sensitive to the reflection angle θ_{XR}. If θ_{XR} tends to 0.3π and the iron abundance tends to about 2 solar value, the implied separation between the two clouds tends to infinity. This information may significantly restrict or even rule out the X-ray reflection model if iron abundance can be measured independently.

Despite the fact the all of the discussed models have limitations, we find that the X-ray reflection model is the most viable. For the X-ray model to work we only need to assume the specific positions of the irradiated clouds. The strongest support is provided by the required timings of the flares for the model to coincide with the values obtained independently. In comparison, models involving charged particles require an additional local particle accelerator located nearby the specific clouds. Although there are some indications of interaction of the Arches cluster with the surrounding molecular gas, it is not clear if there is a shock near the clouds bright in X-rays and if the shock in question is able to provide the necessary power to the charged particles.

However, there are some possible challenges to the X-ray reflection model:

1. The model requires the clouds to be in specific locations. Future observations on the relative distance between the two irradiated clouds will be crucial for the model.
2. The X-ray reflection model predicts that when the second flare leaves the cloud, the intensity of the X-ray emission will start to decrease again. Since we do not know the size of the cloud and the duration of the flare, it is difficult to specify the exact moment of time. However, given the fact that the duration of the flare is of the order of 10 years, this decrease may be observed in the near future. In the frame of CR models, the intensity of X-ray emission should stay constant within 0.5–1.0 of the currently observed values.
3. As we already mentioned, the X-ray reflection model and the proton model are very sensitive to assumed iron abundance. If independent observations show that iron abundance is higher than we used in our calculations, only the electron model will be able to reproduce the observed emission properties.

The authors are grateful to E. M. Churazov for useful suggestions. V.A.D. and D.O.C. are supported in part by the grant RFBR 18-02-00075. D.O.C. is supported in part by the foundation for the advancement of theoretical physics and mathematics "BASIS." R.K. acknowledges support from the Russian Science Foundation (grant 14-22-00271). C.M.K. is supported in part by the Ministry of Science and Technology of Taiwan under grants MOST 104-2923-M-008-001-MY3 and MOST 105-2112-M-008-011-MY3. K.S.C. is supported by the GRF Grant under HKU 17310916.

ORCID iDs

D. O. Chernyshov https://orcid.org/0000-0003-0716-5951
C. M. Ko https://orcid.org/0000-0002-6459-4763
R. A. Krivonos https://orcid.org/0000-0003-2737-5673

References

Baring, M. G., Jones, F. C., & Ellison, D. C. 2000, ApJ, 528, 776
Blumenthal, G. R., & Gould, R. J. 1970, RvMP, 42, 237
Chuard, D., Terrier, R., Goldwurm, A., et al. 2018, A&A, 610, A34
Churazov, E., Khabibullin, I., Sunyaev, R., & Ponti, G. 2017, MNRAS, 465, 45
Clavel, M., Soldi, S., Terrier, R., Tatischeff, V., et al. 2014, MNRAS, 443, L129
Clavel, M., Terrier, R., Goldwurm, A., et al. 2013, A&A, 558, A32
Dogiel, V., Cheng, K. S., Chernyshov, D., et al. 2009, PASJ, 61, 901
Dogiel, V., Chernyshov, D., Koyama, K., et al. 2011, PASJ, 63, 535
Dogiel, V. A., Chernyshov, D. O., Kiselev, A. M., et al. 2015, ApJ, 809, 48
Dogiel, V. A., Chernyshov, D. O., Kiselev, A. M., & Cheng, K. S. 2014, APh, 54, 33
Dogiel, V. A., Chernyshov, D. O., Tatischeff, V., Cheng, K. S., & Terrier, R. 2013, ApJL, 771, L43
Dogiel, V. A., Ichimura, A., Inoue, H., & Masai, K. 1998, PASJ, 50, 567
Haug, E. 1998, SoPh, 178, 341

Hayakawa, S. 1964, in Cosmic Ray Physics, ed. R. E. Marshak, (New York: Interscience Monographs)
Indriolo, N., & McCall, B. J. 2012, ApJ, 745, 91
Koyama, K., Maeda, Y., Sonobe, T., et al. 1996, PASJ, 48, 249
Krivonos, R., Clavel, M., Hong, J., et al. 2017, MNRAS, 468, 2822
Krivonos, R. A., Tomsick, J. A., Bauer, F. E., et al. 2014, ApJ, 781, 107
Nobukawa, K., Nobukawa, M., Koyama, K., et al. 2018, arXiv:1801.07881
Nobukawa, K. K., Nobukawa, M., Uchiyama, H., et al. 2015, ApJL, 807, L10
Nobukawa, M., Ryu, S. G., Tsuru, T. G., & Koyama, K. 2011, ApJL, 739, L52
Ponti, G., Terrier, R., Goldwurm, A., Belanger, G., & Trap, G. 2010, ApJ, 714, 732
Revnivtsev, M. G., Churazov, E. M., Sazonov, S. Y., et al. 2004, A&A, 425, L49
Ryu, S. G., Nobukawa, M., Nakashima, S., et al. 2013, PASJ, 65, 33
Serabyn, E., & Guesten, R. 1987, A&A, 184, 133
Skilling, J., & Strong, A. W. 1976, A&A, 53, 253
Stolte, A., Ghez, A. M., Morris, M., et al. 2008, ApJ, 675, 1278
Sunyaev, R., & Churazov, E. 1998, MNRAS, 297, 1279
Sunyaev, R. A., Markevitch, M., & Pavlinsky, M. 1993, ApJ, 407, 606
Tatischeff, V. 2003, in EAS Publications Ser. 7, Final Stages of Stellar Evolution, ed. C. Motch & J.-M. Hameury (Les Ulis: EDP Sciences), 79
Tatischeff, V., Decourchelle, A., & Maurin, G. 2012, A&A, 546, 88
Terrier, R., Clavel, M., Soldi, S., et al. 2018, A&A, 612, A102
Terrier, R., Ponti, G., Belanger, G., et al. 2010, ApJ, 719, 143
Tsujimoto, M., Hyodo, Y., & Koyama, K. 2007, PASJ, 59, S229
Walls, M., Chernyakova, M., Terrier, R., & Goldwurm, A. 2016, MNRAS, 463, 2893
Wang, Q. D., Dong, H., & Lang, C. 2006, MNRAS, 371, 38
Yusef-Zadeh, F., Hewitt, J. W., Wardle, M., et al. 2013, ApJ, 762, 33
Yusef-Zadeh, F., Law, C., Wardle, M., et al. 2002, ApJ, 570, 665
Yusef-Zadeh, F., Muno, M., Wardle, M., & Lis, D. C. 2007, ApJ, 656, 847
Zhang, S., Hailey, C., Mori, K., et al. 2015, ApJ, 815, 132